



HAL
open science

A novel method of computer based interferogram evaluation

Jiri Olejnicek, Jan Pichal, Josef Blazek, Petr Spatenka

► **To cite this version:**

Jiri Olejnicek, Jan Pichal, Josef Blazek, Petr Spatenka. A novel method of computer based interferogram evaluation. 2004. hal-00001855

HAL Id: hal-00001855

<https://hal.science/hal-00001855>

Preprint submitted on 23 Oct 2004

HAL is a multi-disciplinary open access archive for the deposit and dissemination of scientific research documents, whether they are published or not. The documents may come from teaching and research institutions in France or abroad, or from public or private research centers.

L'archive ouverte pluridisciplinaire **HAL**, est destinée au dépôt et à la diffusion de documents scientifiques de niveau recherche, publiés ou non, émanant des établissements d'enseignement et de recherche français ou étrangers, des laboratoires publics ou privés.

A NOVEL METHOD OF COMPUTER BASED INTERFEROGRAM EVALUATION

Jiří Olejníček^{1,3}, Jan Píchal², Josef Blažek³, Petr Špatenka³

¹⁾ *Institute of Physics, Academy of Sciences of the Czech Republic, Na Slovance 2, Prague, Czech Republic*

²⁾ *Czech Technical University, Faculty of Electrical Engineering, Technická 2, Prague, Czech Republic*

³⁾ *University of South Bohemia, Department of Physics, Jeronýmova 10, Č. Budějovice, Czech Republic*

Abstract:

Paper presents a new alternative procedure for evaluation of interference patterns recording the light beam deflection in cylindrically symmetrical phase objects. Described method is applicable for evaluation of complicated interference patterns containing heavily distorted, double or closed interference fringes, too. Developed algorithm was applied to a complex interference pattern taken in deuterium burning pinch discharge and electron density values in the discharge channel were obtained. Paper also discusses influence of the phase shift deformation outside the region under study on the accuracy of results and on electron density estimation inside the shock wave of the pinch. The calculation of electron temperature in the discharge channel was performed providing kinetic and magnetic pressures equilibrium. All calculations had been performed in the MATLAB computing environment.

Keywords: Interferometry; Delaunay triangulation; Pinch discharge; Electron concentration; Electron temperature

1. Introduction

Optical interferometry is one of non-obtrusive experimental methods applicable for the plasma study. It makes use of the light wave velocity changes during the light wave passing through the medium. The velocity changes are related with the refractive index changes of the medium they are passing through. If it is possible to determine the refractive index changes and compare them with a definite "reference" value, the theoretical models can be used for the calculation of further characteristics.

The study of plasma characteristics by means of optical interferometry makes possible to exclude the problem of plasma interaction with the phase object. Optical interferometry plays on the light ray distortion during its passage through the studied region and its subsequent interference with an "undistorted light". The characteristics under study may be quantities related with or influencing the index of plasma refraction at least to such a degree that the shift related with the plasma refraction changes can be registered in an interferogram. Correlated representative characteristics are e.g. temperature and pressure of neutral gas, concentrations of admixtures with different index of refraction or concentration of free electrons in high-ionised plasma.

Resultant interferogram usually creates distorted system of originally parallel interference fringes. Knowing the fringe shift and assuming the phase object rotational symmetry the distribution of characteristics under investigation can be calculated. Calculation is based [1] on the equation for "distorted" and "undistorted" light wave optical paths difference

$$\delta\varphi = \frac{2\pi}{\lambda_0} \cdot \int [n(x, y, z) - n_0] dr, \quad (1)$$

where $\delta\varphi$ is the phase shift of interfering waves, λ_0 is the light wavelength, n_0 region outside the phase object index of refraction, $n(x, y, z)$ local refractive index of the point with coordinates (x, y, z) in the test zone and dr is light wave path element. The equation (1) is based on condition of light ray straight-line propagation and assuming no light ray deflection.

In this case the phase shift values can be directly read from an interferogram and used for calculation of refractive index distribution. Dependence of the square of the complex refractive index on relevant cyclotron frequencies can be for electromagnetic wave of frequency ω expanding in plasma (plasma frequency ω_p) described by a formula

$$n^2 = 1 - \frac{\omega_p^2}{(\omega - \omega_{c,e}) \cdot (\omega + \omega_{c,i})}, \quad (2)$$

where $\omega_{c,e}$ and $\omega_{c,i}$ are electron and ion cyclotron frequencies. For zero or negligible small external magnetic field intensity values and refractive index being comparable to one the equation (2) can be rewritten for $n \approx 1$ in form

$$n - 1 = -\frac{N_e e^2 \lambda^2}{8\pi^2 \varepsilon_0 m_e c^2} = -4.485 \cdot 10^{-16} \lambda^2 N_e, \quad (3)$$

where N_e is electron density, e charge of electron, ε_0 free-space permittivity, m_e electron mass, λ is the wavelength and c velocity of light.

The equation (3) gives an idea about the refractive index values in case of electromagnetic waves expanding in plasma with electron concentration N_e . It is obvious, that the phase velocity of the wave exceeds the velocity of light, but because the phase velocity is not related with the transfer of information this fact does not contradict the theory of relativity.

Having an interferometer capable of refractive index changes of order 10^{-5} measurement, the application of eq. (3) and the use of visible light (400-650 nm) make determination of electron density values of order 10^{16} cm^{-3} possible.

2. Algorithm for phase shift calculation

Creation of interference fringe bifurcation, fringes “optical” superposition and coinciding and closed fringes formation related with the light beam passage through the region under study, formation of very exotic interference pattern shapes in case of heavily distorting phase objects might occur. The existence of such objects and “irregularities” sets new requirements on the evaluation algorithms and makes the standard evaluation methods more difficult.

Primary task of taken interference pattern evaluation is the estimation of phase shift values in individual points of the interference pattern. Only knowledge of the phase shift values in every pixel of the pattern may lead to knowledge of wanted physical quantity distribution. For demonstration of applicability of our new algorithm and method of interference pattern evaluation we used a complicated interfer-

ence pattern [2] (see Fig. 1) containing all “irregularities” described in previous paragraph.

The fringe pattern in Fig. 1 was taken in the PF 150 coaxial gun equipment of Institute of Plasma Physics and Microfusion in Warsaw, Poland, (inner electrode diameter 5 cm, outer electrode diameter 20 cm, discharge current reached its maximum 0.5 MA about 5 μs after moment of discharge ignition, discharge chamber was filled with deuterium under pressure of 266 Pa) and corresponds to the pinch discharge at the moment of maximum compression. For experiments the Mach-Zehnder interferometer and Nd-YAG laser (531 nm) were used. Typical time of interference pattern registration was about 8 ns. Interference pattern was registered on b/w film.

Original interferogram must be digitally modified before the phase shift subtraction and subsequent evaluation. All regions of „irregularities“ requiring careful and appropriate processing (and proper algorithm) are marked in Fig. 1.

We must be aware, that while the existence of fringe bifurcation (region 1) is really possible in the practice, the superposition and coinciding of fringes (region 2) is a mere optical effect caused by high density of fringes in this region. Formation of closed fringes (region 3) is related with great phase changes and being no commonplace it can occur also in case of finite-width interferograms. Region 4 represents parasitic interference fringes on inner electrode and there is no reason to evaluate them.

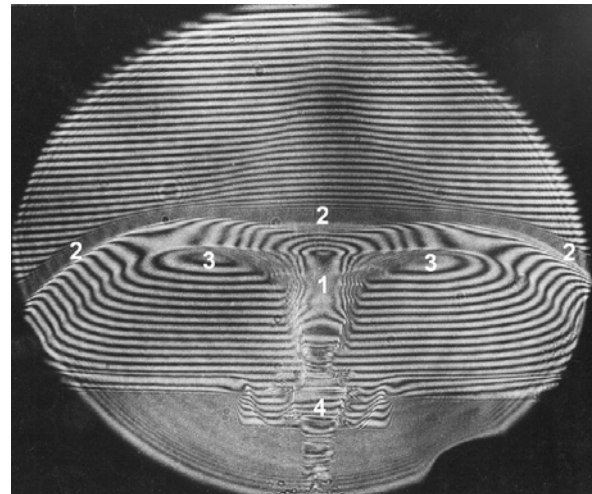


Fig. 1. Interference pattern taken in the pinch discharge (details in text): 1-region of the discharge channel with example of fringes bifurcation, 2-region of the shock wave with example of fringes “optical” superposition and coinciding, 3-region of closed fringes formation, 4- parasitic interference fringes on inner electrode



Fig. 2. Cut of the original interferogram. Final cut dimensions were 523x220 pixels (158x68 mm).



Fig. 3. Cut of the interferogram transferred into the binary code.



Fig. 4. Modified cut with reconstruction of indistinct and double lines.



Fig. 5. Resultant interferogram transferred back into degrees of shade and modified with a Gaussian filter of size 3x3.

Pinch discharge from Fig. 1 burnt upwards from the inner electrode at the bottom of the figure and plasma flow turned aside to the outer electrode lying outside the registered region near the shock wave boundary (2). Our primary task was free electron density determination based on the phase shift and refractive index calculation, therefore we focused on evaluation of regions (1) and (3). Before the phase shift subtraction and subsequent processing the original interferogram had to be digitally modified. Individual steps of this modification were as follows (see Figs. 2-5):

Original interferogram was cut into area of 523x220 pixels corresponding to the final cut dimensions 158x68 mm (Fig. 2). Cut boundaries were chosen in such a way so that lower boundary corresponded to the region where no parasitic interference shift existed and upper boundary had not to trench deeply into the shock wave region, with hardly distinguishable individual fringes. Both area edges were chosen in such a way that resultant area-rectangle contained maximum of complete interference fringes and therefore the most comprehensive information about the phase setting on both sides of the cut.

Chosen interference pattern cut was standardized. Intensity values of individual pixels were in interval $\langle 0,1 \rangle$ and were transferred into the binary bicolour code (Fig. 3).

In next step processed cut image was restored, defective fringes reproduced and parasitic pixels caused e.g. by the interferometer's aberration removed (Fig. 4). Resultant interferogram was transferred back into degrees of shade and modified with Gaussian filter defined by convolution mask given in form of matrix

tion removed (Fig. 4). Resultant interferogram was transferred back into degrees of shade and modified with Gaussian filter defined by convolution mask given in form of matrix

$$h = \frac{1}{16} \begin{bmatrix} 1 & 2 & 1 \\ 2 & 4 & 2 \\ 1 & 2 & 1 \end{bmatrix}. \quad (4)$$

Final version of modified interference pattern cut is in Fig. 5. The cut area of 523x220 pixels was transformed into 600x600 pixels. This reduction did not influence final results, it was important for algorithm used for the interference fringe approximation only.

Phase shift calculation had been performed in the MATLAB computing environment. Evaluation algorithm was as follows: coordinates of a point and relevant phase shift value expressed in multiple of π were entered into the programme. (Multiple of π being even means that interfering rays are shifted just a whole wavelength multiple farther in this point. They are represented with light lines. Multiples of π being odd are represented with dark lines and mean that interfering rays are shifted just a $(2k-1)\lambda/2$ farther in these points.) Algorithm checked surroundings of processed point and then moved into a point with extreme intensity value. For even multiple searched point of maximum intensity, for odd multiple searched point of minimum intensity. Next the programme

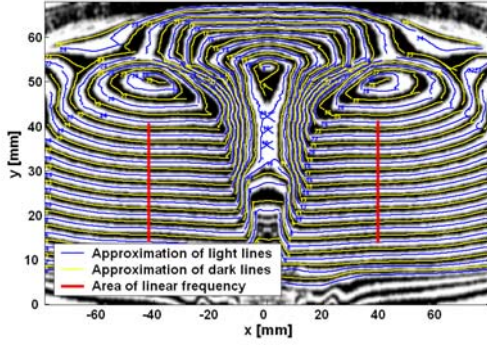


Fig. 6: Original interferogram with approximated equidenses. Vertical straight lines indicate the shiftless region within the investigated area.

shifted in location by one pixel to the left, eventually to the right and checked pixels placed up and under the current pixel in its surrounding and a new position was relocated into the point of extreme intensity. The algorithm repeated itself until the boundary of the interferogram or a predefined position (interval) was reached. For fringes' or parts of fringes' slopes greater than 45° the programme located extreme intensity pixels by another regime – the algorithm moved up, eventually down and located pixels characterized with extreme intensity value in the left or in the right environs of the current point. During every step the programme saved predefined value of the phase shift into the matrix on position corresponding to the actual location of the ascertained pixel. Finally all light and dark interference fringes were approximated by „equidenses“ of extreme intensity points (Fig. 6).

From a mathematical point of view the approximation leads to formation of a sparse matrix containing data „strings“ with phase shift values. To get complete information about the phase shift distribution in all matrix points or at least in points inside the region under study the data from the resultant matrix were 2D cubically

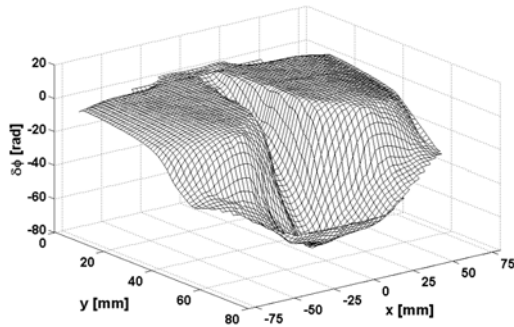


Fig. 8. Resultant phase shift values after subtraction of f_0 .

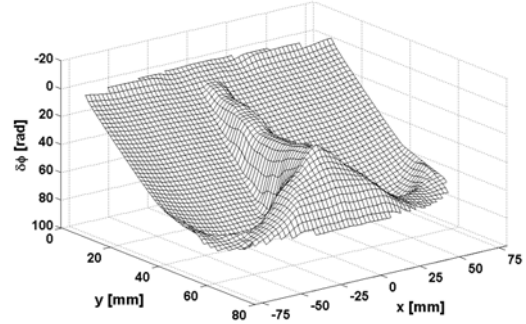


Fig. 7: Phase shift obtained by cubic 2D interpolation of data from previous figure. For better illustration the z-axis direction is turned round.

splined by means of Delaunay triangulation [3, 4]. But in points very near the convex hull of the data the Matlab algorithm making this triangulation returned the NaN values (not a number). These points had to be substituted in next step with simple average of phase shift values of adjoining points. The whole process resulted in a dense continuously defined matrix containing values of the phase shift with introduced space frequency caused by slight decline of interfering rays.

The interference pattern structure in case of the finite width interferogram can be expressed as

$$g(x, y) = a(x, y) + b(x, y) \cdot \cos[2\pi f_0(x, y) + \phi(x, y)], \quad (5)$$

where $a(x, y)$ and $b(x, y)$ are invariables, $\phi(x, y)$ wanted phase shift and $f_0(x, y)$ introduced undesirable space frequency. To get information about the real phase shift, the subtraction of this space frequency is fundamental.

The space frequency subtraction was achieved in following way: a shiftless region within the investigated area was found (see

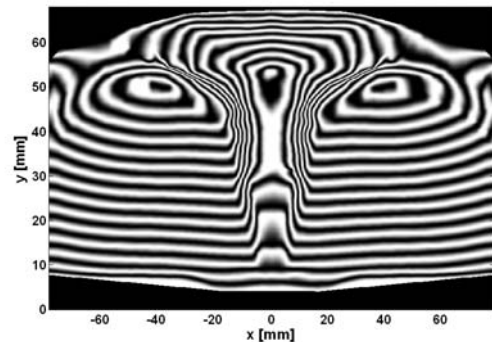


Fig. 9. Model interferogram reconstructed by means of calculated phase shift values from Fig. 7.

Fig. 6, appropriate regions are indicated with vertical lines). Knowing the phase shift values in these regions the original undisturbed interferogram was restored. Should the evaluated regions be mutually phase shifted the original interference fringes had not to be horizontal or equally wide. Obtained interference pattern structure represented introduced undesirable space frequency $f_0(x, y)$ from eq. (5). By subtraction of $f_0(x, y)$ values from values plotted in Fig. 7 we got wanted $\delta\varphi$ values derived in eq. (1) (see Fig.8). Fig. 9 represents model of interference pattern calculated from data shown in Fig. 7. Comparison of both interference patterns (real in Fig. 6 and model in Fig. 9) indicates the accuracy of the computation. More information about model interferograms of this case is possible to find in work [5].

3. Refractive index and electron density calculation

Obtained phase shift distribution had to be converted into refractive index distribution and then using eq. (3) into electron density distribution. Pinch discharge burning between two circularly concentric electrodes showed cylindrical symmetry and therefore the inverse Abel transformation might be used for further calculation. The Abel transformation is generally defined by

$$n_r - n_0 = \int_r^R \frac{dD/dx}{\sqrt{x^2 - r^2}} dx, \quad (6)$$

where n_r is refractive index value in distance r from the symmetry axis, n_0 is refractive index value outside the region under study, R outer radius of the evaluated region with the phase object interaction and D “interference order”. For numerical processing and discrete phase

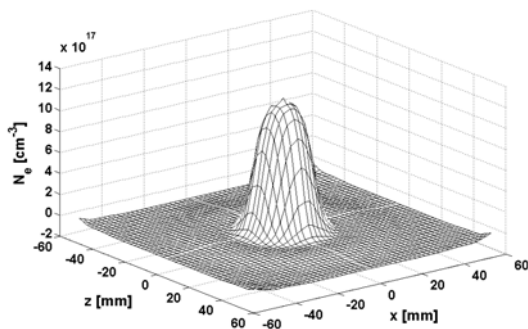


Fig. 10. Space distribution of electron density for $y = 40\text{mm}$

shift values the evaluation based on eq. (6) can be modified in more suitable form. Let us imagine the phase shift map as cylindrically symmetric object and split it in k concentric annuli each with constant index value. The eq. (6) can be transformed into system of equations with simply numerical solution

$$\delta\varphi_i = \frac{4\pi}{\lambda_0} \cdot \Delta r \cdot \sum_{j=1}^i \Delta n_j \cdot A_{ji}, \quad (7)$$

where

$$A_{ji} = \sqrt{(k-j+1)^2 - (k-i)^2} - \sqrt{(k-j)^2 - (k-i)^2} \quad (8)$$

$\delta\varphi$ is the phase shift of the “ i -th” ray, i.e. of beam passing through the 1st, 2nd, . . . j -th outer annulus, Δr width of any annulus, λ_0 is the light wavelength in the shiftless region and products $\Delta r A_{ji}$ are elements of path which the i -th ray covered by the passage through the j -th annulus. Concrete values were derived from characteristics of evaluated interference pattern: k corresponded to a half width of evaluated pattern, i.e. it was equal to = 300 (each annulus corresponded to the form of one pixel the interferogram), $\Delta r = 0.263\text{mm}$ (the annulus width equaled to x dimension of one pixel) and $\lambda_0 = 531\text{ nm}$ (wavelength of the Nd-YAG laser second harmonic). Calculation proceeded from the outer annulus inwards to the symmetry axis and refractive index distribution along the phase shift object radius was determined.

Knowing the refractive index distribution and eq. (3) the electron density distribution profile in the discharge channel was calculated. Results for various y -coordinates can be seen in figures 10 and 11.

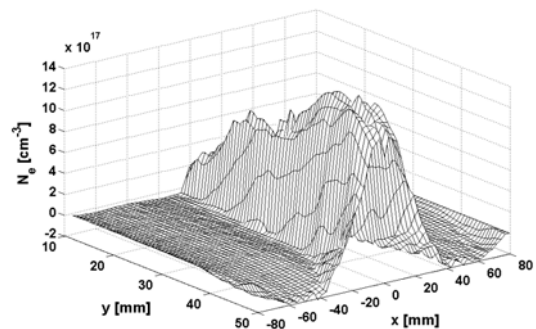


Fig. 11. Electron density distribution in the discharge channel.

4. Phase shift deformation outside region under study and accuracy of the calculation

All results presented in previous graphs were obtained providing that no interference pattern (and passing laser beam) deformation outside the region under study, i.e. outside evaluated interference pattern cut (see Fig. 2) would occur. But this assumption was not fully valid (see Fig. 1) and discussion of relation between this deformation and accuracy of results was necessary. Although the inverse Abel transformation equations are not too sensitive to boundary condition changes, i.e. to the phase shift changes outside evaluated region, nevertheless it is recommendable to verify this ascertainment in every individual case with computing.

Graph 13 demonstrates the refractive index (and of course electron density distribution calculated for points at the symmetry axis) changes in dependence on zero phase shift zone position (Fig 12), or in case of region closely adjacent to the zero phase shift zone elimination. Graphs 12 and 13 explicitly show almost negligible influence of the in cut diversely adjusted zero phase shift zone on the accuracy of results – about 15%. Change of the phase shift profile of order about -25 rad at the symmetry axis corresponds to the refractive index change of about $-2 \cdot 10^{-5}$ (see Fig. 14). This change is almost non-measurable. It can be shown, that amplitude of this change did not depend on the phase shift profile shape, but it depended only on the shift (and the annulus width Δr) magnitude. Be phase profiles difference appointed as σ , the phase profiles $\delta\varphi$ (solid line from Fig. 12) and $\delta\varphi'$

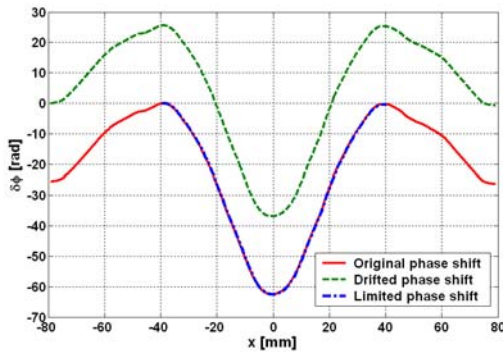


Fig. 12. Phase shift for $y = 50$ mm. Solid line: zero phase shift level was assigned to the phase shift maximum value. Dashed line: zero phase shift level was assigned to the phase shift profile left edge. (The same condition was used in Figs. 10 and 11). Dot and dashed line: Edge data were eliminated and zero phase shift level was assigned to the phase shift maximum value of rest data.

(dashed line from Fig. 12) can be defined as

$$\delta\varphi = \delta\varphi' + \sigma. \quad (9)$$

Note, that $A_{jk}=1$ for all terms A_{jk} from eq. (7) and any j . Hence the total error of the calculated refractive index values at the symmetry axis is

$$\Delta n'_k - \Delta n_k = \frac{\lambda_0 \sigma}{4\pi \Delta r} - \sum_{j=1}^{k-1} (\Delta n'_j - \Delta n_j), \quad (10)$$

The sum on the right side of eq. (10) can be rewritten as (δ_j is excluded):

$$\sum_{j=1}^{k-1} (\Delta n'_j - \Delta n_j) = \frac{\sigma \lambda_0}{4\pi \Delta r} \cdot \left(\begin{aligned} & \frac{1}{A_{11}} + \frac{1}{A_{22}} - \frac{A_{12}}{A_{11}A_{22}} + \\ & + \frac{1}{A_{33}} - \frac{A_{13}}{A_{11}A_{33}} - \frac{A_{23}}{A_{22}A_{33}} + \frac{A_{12}A_{23}}{A_{11}A_{22}A_{33}} + \dots \end{aligned} \right) \quad (11)$$

The curve of computed refractive index values difference, i.e. difference of distributions from Fig. 13 is plotted in Fig. 14. Nevertheless the curve in Fig. 14 corresponds to the difference caused by the shock wave “echo” at interference pattern cut edges only. The cut selection was chosen in the way minimizing both the echo and deformation of parallel interference fringes outside of the burning discharge channel.

Real influence of the total deformation in the outside region must be comprehend into

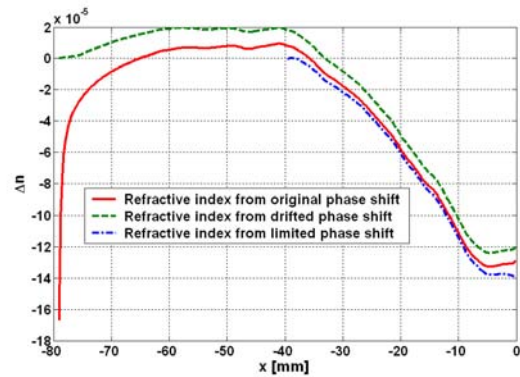


Fig. 13. Refractive index distribution calculated from data plotted in previous figure. Types of lines were kept. Maximum value of difference of refractive index in plasma discharge channel at the symmetry axis was $2 \cdot 10^{-5}$. It represents error approximately 15%.

computation. That is why we integrated the fringe structure inside the shock wave into already for computation used interference pattern, see Fig. 15. The cut covers left side of the evaluated interference pattern only, but its x -dimension is 122 mm, i.e. it is about 43 mm longer than dimension of initially evaluated pattern cut from Fig. 2 if you like Fig. 6.

At least one y -profile must crosscut entire modified interference pattern to obtain complete phase shift profile, an example of a proper y -profile is shown by dotted line in Fig. 15 and 17.

Modified pattern is processed with the same algorithm as described in sec. 2, the only difference is the omission of odd π multiples, but due to a high density of interference fringes it almost does not influence the accuracy of computing.

Parameters of inverse Abel transformation computation were also changed. New processed matrix was 900x652 pixels, i.e. new $k = 900$ and new annulus width $\Delta r = 0.136$ mm. Used laser wavelength λ_0 remained unchanged. Resultant phase shifts are presented in Figs. 16 and 17.

Both phase profiles along y -crosscut are

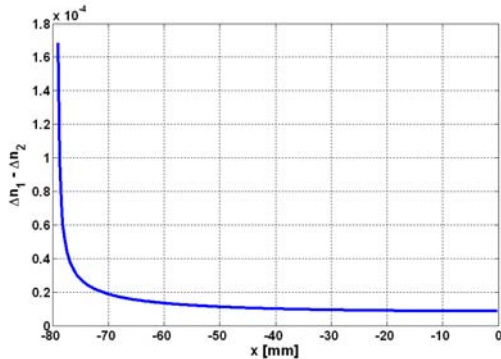


Fig. 14. Difference of computed refractive index values from Figs. 13 and 21.

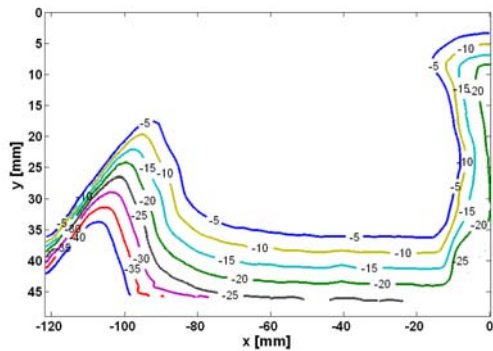


Fig. 16. Area with computed phase shift in radians calculated from interference pattern in Fig. 15.

shown in Fig. 18 and corresponding refractive index difference distribution in Fig. 19.

Due to easy shock wave influence determination the zero phase shift zone position was identical in both cases – with and without shock wave implementation. Corresponding electron density and electron density difference distribution present Figs. 20 and 21.

It is remarkable that resultant electron density difference in points at symmetry axis was about $2,5 \cdot 10^{16} \text{ cm}^{-3}$. This mistake represents about 5% of electron density total value ($5,5 \cdot 10^{17} \text{ cm}^{-3}$). Similar interferometric measurements typical accuracy is about 20%, therefore 5% mistake introduced by the computation boundary condition choice is negligible small. It must be emphasized that evaluated cut on the left side of the pattern did not involve entire phase shift decrease. True value of phase shift decrease could be only hardly estimated without knowledge of the interference structure outside on interferogram taken region.

Should the $\delta\varphi_1$ value used in the start of the algorithm be smaller than shape shown in Fig. 18 (and it is the case), both curves in graphs in Figs. 19 and 20 would be more identical. This equality can be explained also from physical

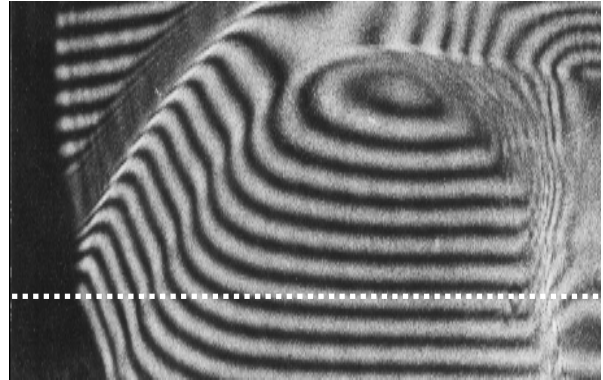


Fig. 15. Modified interference pattern with reconstructed interference fringes inside the shock wave. Dotted line indicates the crosscut used for calculation. Area of this enlarged cut is 122x49 mm.

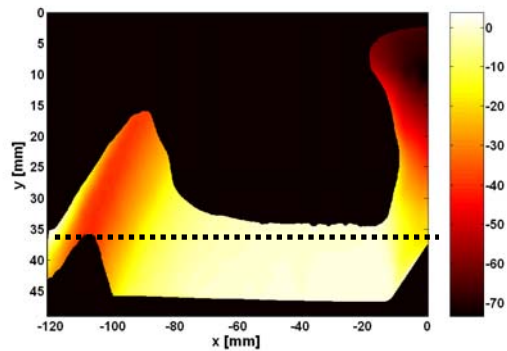


Fig. 17. Phase shift in radians from Fig. 16 after space frequency subtraction.

point of view – due to its great radius (about six times greater than discharge channel radius) the shock wave acts for laser beams passing perpendicularly through the object under study as plane parallel plate almost equally deforming all rays and therefore it does not influence the phase shift relative value in the central region. Nevertheless this relative phase shift is crucial for measured quantities computation. But for great values of y this assumption is not valid any more. With growing y the shock wave radius reduces together with fast changes of the angle between shock wave and light rays. For great y values precise explanation of the interference fringes deformation is very difficult, i.e. having incomplete interference pattern and no possibility to distinguish number of interference fringes hidden inside the shock wave it is impossible.

5. Electron temperature calculation

Electron temperature calculation had been performed for illustration of other discharge parameters only. By means of electron density computation described in previous paragraph the electron temperature computation was

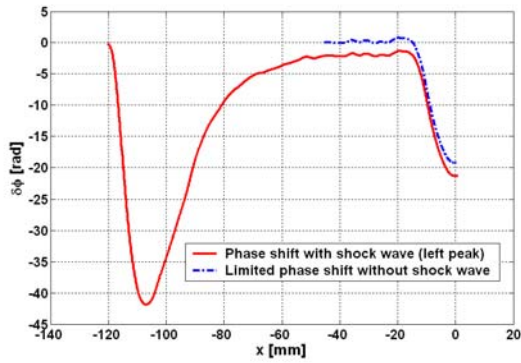


Fig. 18: Phase shifts calculated along y -coordinate crosscut from Fig. 15.

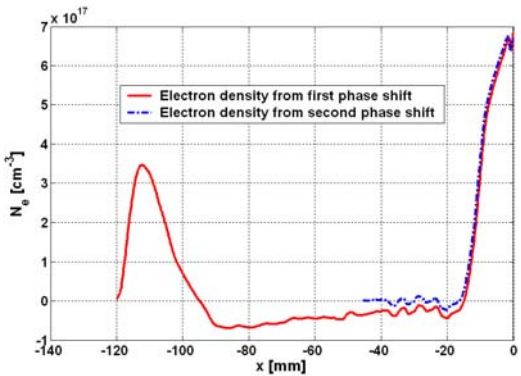


Fig. 20: Electron density distributions consistent with distributions from Fig. 19.

only little related with interference pattern evaluation procedure itself.

In state of equilibrium after discharge channel formation the inner kinetic pressure p_k equals to the sum of partial electron and ion pressures

$$p_k = N_e k T_e + \sum_i N_i k T_i, \quad (12)$$

k is the Boltzmann constant, N_i and T_i being i^{th} ion density and temperature. Inner kinetic pressure is compensated by magnetic field induced inside the discharge. Magnetic pressure can be expressed [6] as

$$p_m(r) = -\frac{\mu I^2}{4\pi R^2} \left(1 - \frac{r^2}{R^2}\right), \quad (13)$$

where I is total discharge current, r distance to the discharge channel axis and R discharge channel radius. For two component plasma satisfying $N_e = N_i$ and $T_e = T_i$ the relationship between electron temperature T_e , mean electron density \bar{N}_e , total discharge current and discharge channel radius can be derived by averaging over the whole discharge channel area.

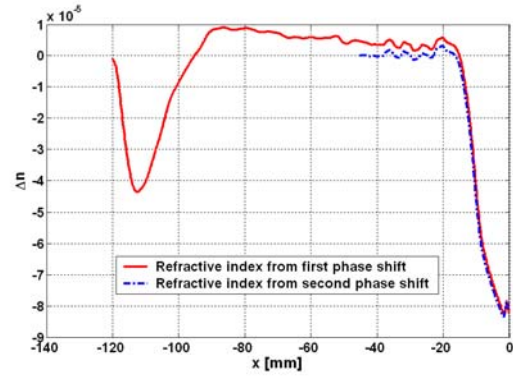


Fig. 19: Refractive index distribution corresponding to phase shifts from Fig. 18.

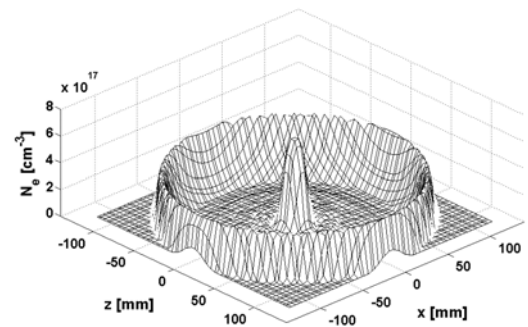


Fig. 21: 3D graph of electron density distribution with shock wave.

$$T_e = \frac{\mu I^2}{16\pi^2 k \bar{N}_e R^2}, \quad (14)$$

Substitution of previous results in eq. (14) resulted in electron density estimation. e.g. for electron density distribution shown in Fig. 10, corresponding to phase profiles along $y=40$ mm and for $I = 0.5$ MA, $\bar{N}_e = 4.08 \cdot 10^{17}$ cm⁻³ and $R=2.05$ cm the electron temperature was $T_e=72$ eV.

Described procedure of electron temperature acquisition is not sensitive to the accuracy of radius R determination. Mean electron density was calculated as integral over total cut area, electron density outside the discharge channel was zero, hence the product $\bar{N}_e R^2$ is directly proportional to the total sum of free electrons in the area of diameter R , i.e. $\bar{N}_e r^2 = \text{const.}$ for $r \geq R$.

For $y \in \langle 30, 40 \rangle$ mm calculated electron temperatures 70–140 eV are in a good agreement with results from [7].

6. Conclusions

Interference pattern digitising and computer processing is quite necessary in modern interferometry. Paper presents a new evaluation method based on simple algorithm applicable for any interference pattern regardless of its width or rate of fringe deformation. The method is appropriate also for evaluation of complicated interference patterns containing heavily distorted, double or closed interference fringes. In spite of the fact that the computer program for phase shift and refractive index computation was written in the MATLAB, the use of this computing environment is no necessary condition for algorithm successful implementation. The MATLAB was chosen especially due to its excellent ability of operation with matrices representing interference pattern and excellent graphic output. Any other programming language can be of the same usability for experienced programmer.

For algorithm functionality verification a complex pinch discharge interference pattern taken in the PF 150 coaxial gun of Institute of Plasma Physics and Microfusion in Warsaw, Poland was used. Interference pattern given to us by courtesy of IPPMM staff [2] contains almost all in text described “irregularities”. The computation focused both on determination of electron density distribution along the main discharge

channel axis and on electron temperature calculation based on equilibrium of kinetic and magnetic pressures. Obtained values are in a good agreement with our expectation and with results measured in other laboratories.

Acknowledgements:

This research has been supported by the grant MSM 124100004 and by the project LN00A015 of the MŠMT ČR.

References:

- [1] Y.I.Ostrovskii, G.B. Ostrovskaya, M.M.Butusov: Holographitcheskaya interferometria, Nauka Publishers, Moscow 1977. (in Russian)
- [2] by courtesy of M.Paduch and K. Tomaszewski: IPPLM, Warsaw, Poland.
- [3] National Science and Technology Research Center for Computation and Visualisation of Geometric Structures (The Geometry Center), University of Minnesota 1993.
- [4] S.V. Sloan: A fast algorithm for generating constrained Delaunay triangulations, Computers & Structures, Vol. 47 (3): 441-450, 1993.
- [5] J. Olejníček, J. Píchal, J. Blažek, J. Špatenka: An alternative method of interferogram evaluation and processing, Czechoslovak Journal of Physics, Vol. 54 (2004) Suppl. C 349-358
- [6] Kubeš, Pulsní silnoproudé výboje a jejich diagnostika, Prague 1997 (in Czech)
- [7] S. L. Jackson: Holographic interferometry on the ZaP Flow Z-Pinch, University of Washington 2003

Contact:

Jiří Olejníček
 Institute of Physics, Academy of Science of the Czech Republic, Division of Optics
 Na Slovance 2, 182 21 Prague, Czech Republic
 Tel: +420 266 05 2127
 Email: olejn@fzu.cz